Joint Spectral Image Reconstruction for Y-90 SPECT with Multi-Window Acquisition

Minh Phuong Nguyen, Hanvit Kim, Se Young Chun*, Jeffrey A. Fessler, and Yuni K. Dewaraja

***Abstract*—Image reconstruction for Y-90 SPECT is challenging due to wide continuous energy spectrum of the bremsstrahlung photons. Previously, forward projection models with narrow single-energy window or wide multi-energy windows were used for image reconstruction with a single acquisition window. We propose a new Y-90 SPECT image reconstruction method referred to as joint spectral reconstruction (JSR) using multi-energy window forward model and multiple acquisition windows.**

Monte Carlo (MC) simulation using SIMIND coupled with XCAT phantom (two tumors with 80, 41 mL) generated two sets of 6 acquisition window measurements (narrow window: 105-135, 135-165, 165-195, 195-225, 225-255, 255-285 keV, and wide window: 100-200, 200-300, 300-400, 400-500, 500-600, 600-700 keV). Each measurement was scaled to the count level of a typical patient bremsstrahlung SPECT scan following Y-90 microsphere radioembolization of the liver. 3D OSEM with 6 window data and a single image was implemented with 6 energy-dependent collimator detector response, attenuation, and known scatter and was run with 100 iterations, 6 subsets. The reconstructed image was evaluated using the recovery coefficient (RC), the standard deviation (SD), the bias over tumors and liver. Results were compared with those of the single spectral reconstruction (SSR) method that models the projector with a single-energy window with a single acquisition window (105-135 keV for narrow case, and 100-200 keV for wide case).

JSR yielded significantly higher RC and lower SD than SSR in all cases. For narrow window case, JSR achieved up to 11.19% increase in RC and up to 46.9% decrease in SD compared to SSR at the 100th iteration. For wide window case, JSR achieved up to 19.23% increase in RC and up to 19.01% decrease in SD compared to SSR at the 100th iteration. Therefore, our JSR was able to considerably improve Y-90 SPECT image reconstruction quality over SSR. The improvement in noise while maintaining comparable RC is particularly significant because the sensitivity of Y-90 SPECT is low and count levels for applications in targeted radionuclide therapy are low.

***Index Terms*—Yttrium-90, bremsstrahlung, SPECT, reconstruction, joint spectral.**

I. Introduction

YTTRIUM-90 (Y-90) is commonly used in targeted radionuclide therapy. Post-therapy quantitative imaging of the pure beta emitter via bremsstrahlung SPECT has recently gained interest since it allows confirmation of the delivered absorbed dose and implementation of further treatment when needed. Improving the quality of Y-90 imaging by bremsstrahlung SPECT/CT is desirable because of its lower cost and wider availability compared to imaging of Y-90 by state-of-the-art PET/CT. Y-90 SPECT/CT is also more widely applicable including in systemic therapies such as radioimmunotherapy where activity uptake in tumor is relatively low and Y-90 PET is not feasible due to the low probability of the Y-90 positron signal. However, image reconstruction for Y-90 SPECT is challenging due to wide continuous energy spectrum of the bremsstrahlung photons (0-2.3 MeV). This wide spectrum was ignored in past and a narrow energy window, such as 105-195 keV [1], was chosen for reconstruction. Because bremsstrahlung photon generation in tissue is an inefficient process ($<2\%$ of beta interactions in tissue-like material results in photons >50 keV [2]), it is desirable to include as many of the photons as possible.

Recently, there have been some research work dealing with continuous energy ranges in Y-90 image reconstruction [3], [4]. Rong *et al.* proposed to use a forward projection model to incorporate 4 energy windows with energy-dependent collimator detector response (CDR), attenuation, and scatter (ESSE) [3]. Elschot *et al.* proposed to use a fast Monte Carlo (MC) simulator as a forward projection in the reconstruction with 8 energy windows [4]. These methods improved the image quality of Y-90 SPECT significantly. Elschot *et al.* also compared their new Y-90 SPECT with Y-90 time-of-flight-PET and showed comparable results. In the previous two works, even though multi-energy was modeled inside the forward projector, only a single-energy window acquisition window was selected based on trade-offs between several factors.

Exploiting the recent commercial availability of multi-window and list-mode acquisition SPECT systems, in this work we propose a new Y-90 SPECT image reconstruction method that uses the multi-energy window measurements to improve the image quality further.

II. Methods

The statistical image reconstruction of a Y-90 distribution, denoted by $\boldsymbol{f}$, from its measurement data, denoted by $\boldsymbol{y}$, can be obtained by performing the following constrained optimization problem:

$$\hat{\boldsymbol{f}} = \underset{\boldsymbol{f} \geq \boldsymbol{0}}{\arg\max}\, \boldsymbol{L}\left(\boldsymbol{y}|\boldsymbol{f}\right) \tag{1}$$

where $\boldsymbol{L}$ is a Poisson log-likelihood function, defined as:

$$\boldsymbol{L}\left(\boldsymbol{y}|\boldsymbol{f}\right) = \sum_i y_i \log \bar{y}_i\left(\boldsymbol{f}\right) - \bar{y}_i\left(\boldsymbol{f}\right) \tag{2}$$

This research was supported in part by Basic Science Research Program through the National Research Foundation of Korea (NRF) funded by the Ministry of Science, ICT & Future Planning (NRF-2014R1A1A1007928), Republic of Korea, and in part by NIH grant 2RO1 EB001994, USA.

M. P. Nguyen, H. Kim, and S. Y. Chun are with the School of Electrical and Computer Engineering, Ulsan National Institute of Science and Technology (UNIST), Republic of Korea. (*Email: sychun@unist.ac.kr)

J. A. Fessler is with the Department of Electrical Engineering and Computer Science, University of Michigan, Ann Arbor, MI 48109 USA.

Y. K. Dewaraja is with the Department of Radiology, University of Michigan, Ann Arbor, MI 48109 USA.

978-1-4673-9862-6/15/$31.00 ©2015 IEEE

where $\bar{y}_i$ is the mean of y_i - the ith element of the measurement $\boldsymbol{y}$.

We simulated two sets of Y90 bremsstrahlung SPECT measurements with 6 energy windows (narrow and wide windows) that are indexed $e = 1, \ldots, 6$, for each set. We model the measurement for one energy window as

$$\boldsymbol{y}_e \sim \text{Poisson}\left(\boldsymbol{A}_e \boldsymbol{f}_e + \boldsymbol{s}_e\right). \tag{3}$$

where e is an index for energy window, $\boldsymbol{y}_e$ is a measurement for energy window e; $\boldsymbol{A}_e$ is a forward projector for energy window e with energy-dependent CDR and attenuation at the center of energy window e; $\boldsymbol{f}_e$ is an activity distribution in single-energy window e; $\boldsymbol{s}_e$ denotes a mean scatter for energy window e.

We call reconstructing $\boldsymbol{f}_1$ from $\boldsymbol{y}_1$ the single spectral reconstruction (SSR), where the measurement and scatter are selected from the first energy window, and the projector is modeled with a single-energy window.

We propose a joint spectral reconstruction (JSR) method that reconstructs a single activity image from all energy windows data with the following measurement model:

$$\begin{bmatrix} \boldsymbol{y}_1 \\ \vdots \\ \boldsymbol{y}_6 \end{bmatrix} \sim \text{Poisson}\left(\begin{bmatrix} \alpha_1 \mathbf{A}_1 \\ \vdots \\ \alpha_6 \mathbf{A}_6 \end{bmatrix} \boldsymbol{f} + \begin{bmatrix} \boldsymbol{s}_1 \\ \vdots \\ \boldsymbol{s}_6 \end{bmatrix} \right). \tag{4}$$

where we model that $\boldsymbol{f}_e = \alpha_e \boldsymbol{f}$ with α_e obtained by measuring the ratio of the primary counts of window e to the primary counts of window 1. This joint model is similar to the model for motion-compensated image reconstruction using multiple motion frames in [5].

Energy and depth-dependent CDR was obtained from point source MC simulation with high energy collimator, then fitted using B-spline template for the last 3 wide windows and Gaussian model for the rest [6]. Energy-dependent attenuation was obtained by rescaling CT image for energy level of the center of each energy window e. Scatter was assumed to be known in these studies, but one can obtain the scatter contribution using MC scatter estimation methods [7].

MC simulation using SIMIND [8] coupled with XCAT phantom [9] was used to generate clinically realistic data (narrow window: 105-135, 135-165, 165-195, 195-225, 225-255, 255-285 keV and wide window: 100-200, 200-300, 300-400, 400-500, 500-600, 600-700 keV) corresponding to patient studies of Y-90 microsphere (glass) radioembolization in liver malignancies. Two lesions of size 80 mL (Tumor 1) and 41 mL (Tumor 2) were simulated in the liver with activity concentration ratio of liver:tumor:lung, 20:100:1. Before the addition of Poison noise the projection data were scaled to the count level typical for a 30 min Y-90 SPECT scan performed at our clinic after a radioembolization procedure with around 3 GBq of Y-90. SPECT reconstruction was done using the ordered-subsets expectation-maximization (OSEM) algorithm [10] with up to 100 iterations, 6 subsets.

Reconstructed images were evaluated based on recovery coefficient (RC), standard deviation (SD), and bias within a region of interest (ROI) on a tumor or healthy liver (liver part not containing any tumor) calculated as in (5-7). For tumor, ROI is its whole area, and for healthy liver, ROI is a sphere area on the liver, away from tumors to avoid spill-out effect.

$$\text{RC} = \frac{\text{measured count in ROI}}{\text{true count in ROI}} \tag{5}$$

$$\text{SD} = \frac{1}{\bar{\boldsymbol{f}}_{\text{ROI}}} \sqrt{\frac{1}{N-1} \sum\nolimits_{i \in \text{ROI}} \left(\hat{\boldsymbol{f}}\left[i\right] - \bar{\boldsymbol{f}}_{\text{ROI}} \right)^2} \tag{6}$$

$$\text{Bias} = \frac{1}{N} \sum\nolimits_{i \in \text{ROI}} \left| \hat{\boldsymbol{f}}_{\text{noiseless}}\left[i\right] - \boldsymbol{f}_{\text{true}}\left[i\right] \right| \tag{7}$$

The true image, $\boldsymbol{f}_{\text{true}}$, was created using the masks and known activity concentration ratio of liver, tumor, and lung, and scaled to have the same activity level as $\boldsymbol{f}_1$. N is the number of pixels in ROI. $\bar{\boldsymbol{f}}_{\text{ROI}}$ is the average of $\hat{\boldsymbol{f}}$ calculated in ROI. $\hat{\boldsymbol{f}}_{\text{noiseless}}$ is the image reconstructed from noiseless data. $\boldsymbol{f}[i]$ is the ith element of $\boldsymbol{f}$.

III. Results

Fig. 1 shows the normalized CDR profiles for the measurement and corresponding fitting method. For low energy windows (narrow windows: $e = 1, \ldots, 6$, and wide windows: $e = 1, \ldots, 3$), Gaussian fitting is sufficient to match the measured CDR values. However, for high energy windows (wide windows: $e = 4, \ldots, 6$), B-spline template fitting [6] is needed to yield the accurate fit for the obvious penetration tails on the CDR.

A. Results for Narrow Windows

Fig. 2 compares RC, SD, and Bias obtained by JSR and SSR. Significantly higher RC values and lower SD using JSR were observed compared to using SSR for both ROIs. These improvements tend to become much larger as the iteration number increases. At the 100th iteration, JSR yielded up to 11.2% increase in RC and up to 46.9% decrease in SD compared to SSR. These improvements in RC and SD illustrate the advantage of using multiple acquisition windows. In terms of bias, however, JSR was not as good as SSR, which can be explained that using smaller amount of data in SSR can generally achieves the lower bias. Fig. 4 LEFT shows that the visual image quality of the reconstructed image using JSR is better than that using SSR.

TABLE I
PERCENTAGE AT WHICH EACH MEASURE AT THE 100th ITERATION INCREASES WHILE CHANGING FROM SSR TO JSR (NARROW WINDOWS).

	RC	SD	Bias
Tumor1 (80 mL)	2.91	-32.6	14.14
Tumor2 (41 mL)	11.19	-46.9	11.19
Liver	2.06	-38.27	29.99

B. Results for Wide Windows

For wide window case (Fig. 3), the same trends as in narrow window case were obtained for both RC, SD, and Bias. The improvement was relatively higher in RC, but lower in SD. At the 100th iteration, JSR yielded up to 19.23% increase in RC and up to 19.01% decrease in SD compared to SSR.

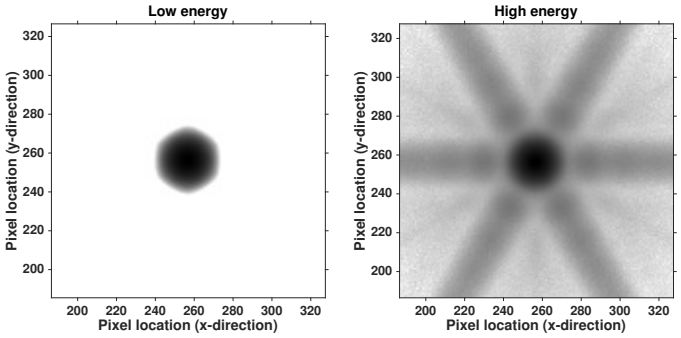

(a) Example of MC simulated CDR

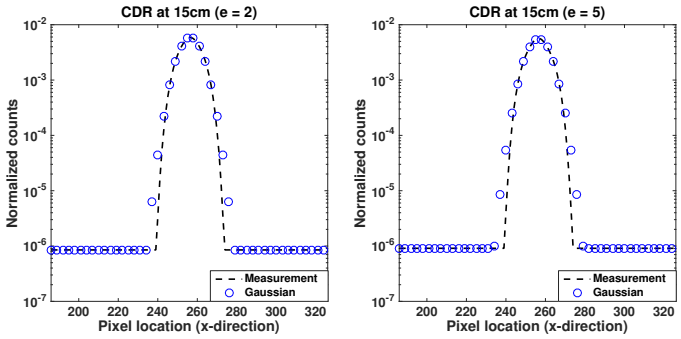

(b) Fitting CDR (Narrow window)

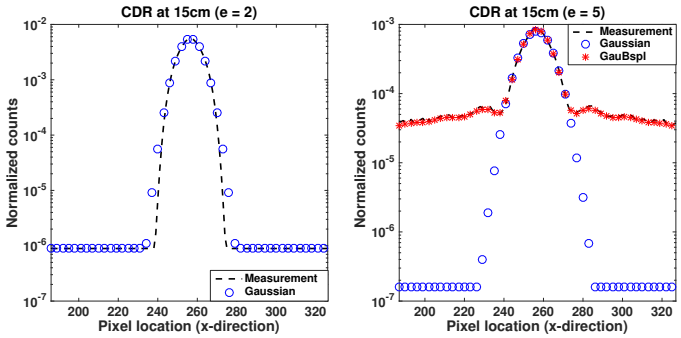

(c) Fitting CDR (Wide window)

Fig. 1. MC simulated and fitted CDR using Gaussian/B-spline (all in log scale).

TABLE II
PERCENTAGE AT WHICH EACH MEASURE AT THE 100th ITERATION INCREASES WHILE CHANGING FROM SSR TO JSR (WIDE WINDOWS).

	RC	SD	Bias
Tumor1 (80 mL)	18.19	-14.36	25.74
Tumor2 (41 mL)	19.23	-9.53	21.28
Liver	14.52	-19.01	74.19

IV. CONCLUSION

JSR with multiple energy window models and acquisition windows considerably improved the Y-90 SPECT image reconstruction quality over SSR. The improvement in noise demonstrated here is particularly significant because bremsstrahlung photon production in tissue is inefficient and SPECT count levels can be low, especially in systemic therapies with Y-90. Further evaluations of the proposed method

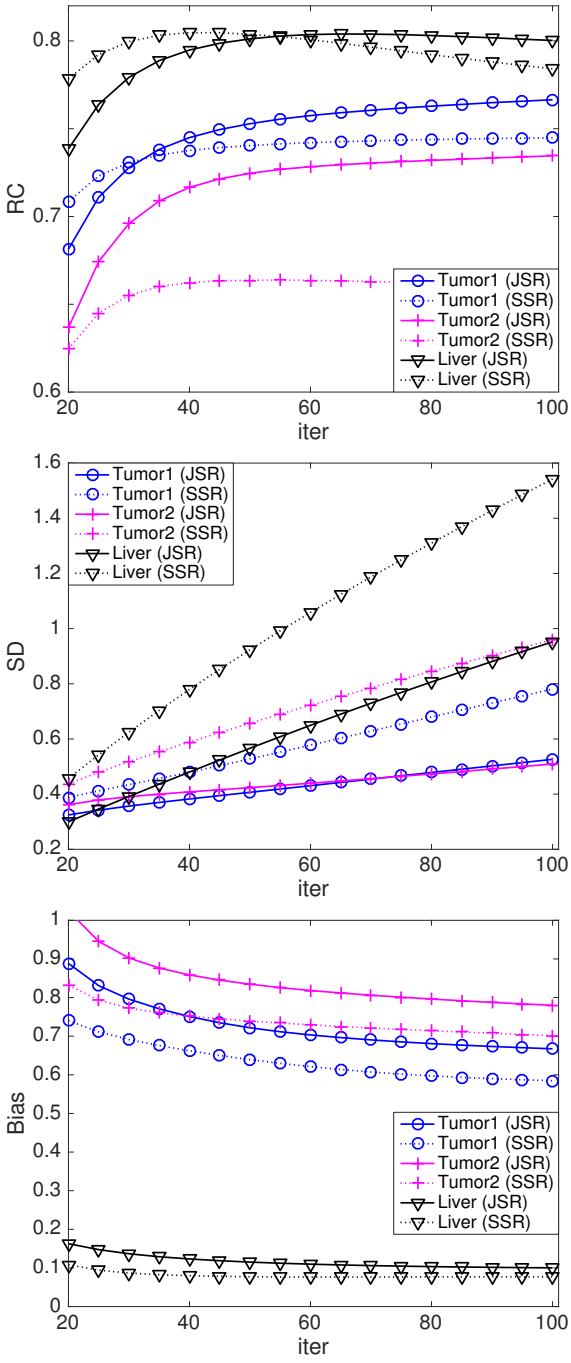

Fig. 2. RC, SD, and Bias for narrow window case.

will be performed with different distributions and tumor sizes in radioembolization as well as in systemic Y-90 therapies. Different energy ranges and widths for the acquisition windows will also be evaluated. Comparison of the proposed method with [3], [4] will be performed in the near future.

REFERENCES

[1] David Minarik, K Sjögreen Gleisner, and Michael Ljungberg, "Evaluation of quantitative 90y spect based on experimental phantom studies," *Physics in medicine and biology*, vol. 53, no. 20, pp. 5689, 2008.

[2] CF Unbe, PL Esquinas, H Piwowarska-Bilska, D Pawlak, R Mikolajczak, B Birkenfeld, and A Celler, "Characteristics of brems strahlung emissions from radionuclide therapy isotopes," in *Nuclear Science*

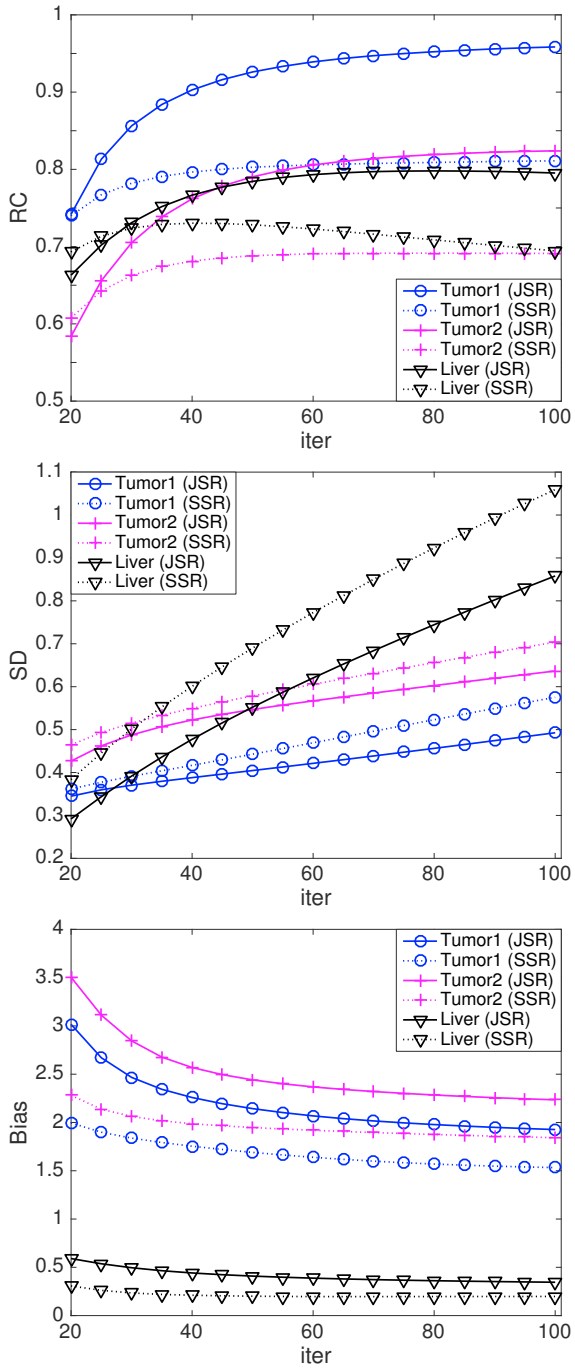

Fig. 3. RC, SD, and Bias for wide window case.

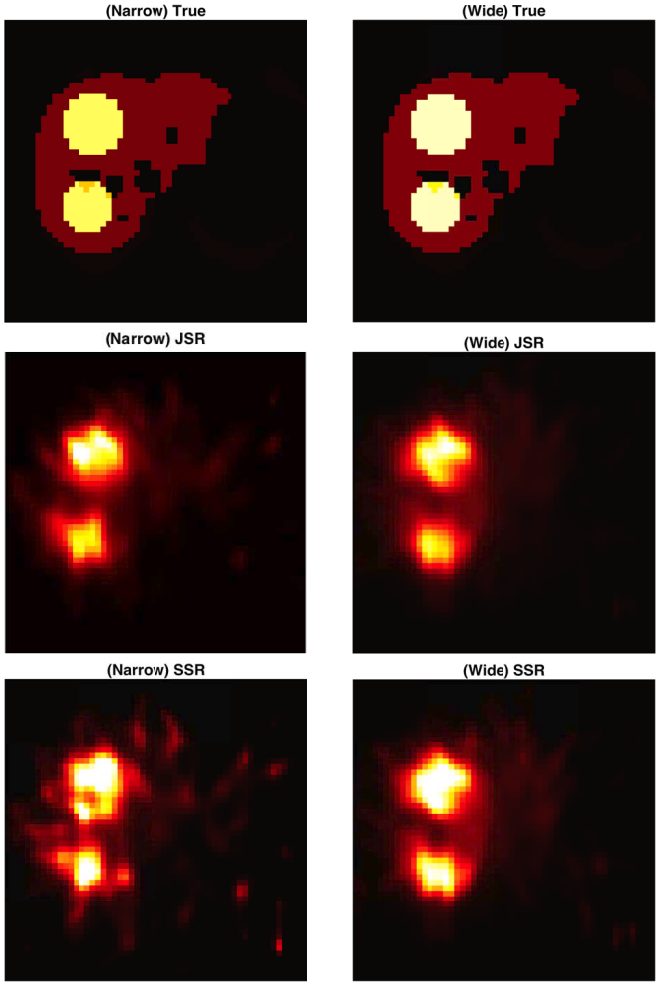

Fig. 4. True and reconstructed images at 35 iteration for narrow and wide window cases.

Symposium and Medical Imaging Conference (NSS/MIC), 2013 IEEE. IEEE, 2013, pp. 1–3.

[3] Xing Rong, Yong Du, Michael Ljungberg, Erwann Rault, Stefaan Vandenberghe, and Eric C Frey, "Development and evaluation of an improved quantitative 90y bremsstrahlung spect method," *Medical physics*, vol. 39, no. 5, pp. 2346–2358, 2012.

[4] Mattijs Elschot, Marnix GEH Lam, Maurice AAJ van den Bosch, Max A Viergever, and Hugo WAM de Jong, "Quantitative monte carlo–based 90y spect reconstruction," *Journal of Nuclear Medicine*, vol. 54, no. 9, pp. 1557–1563, 2013.

[5] Se Young Chun and Jeffrey Fessler, "Noise properties of motion-compensated tomographic image reconstruction methods," *Medical Imaging, IEEE Transactions on*, vol. 32, no. 2, pp. 141–152, 2013.

[6] Se Young Chun, Jeffrey Fessler, and Yuni K Dewaraja, "Correction for collimator-detector response in spect using point spread function template," *Medical Imaging, IEEE Transactions on*, vol. 32, no. 2, pp. 295–305, 2013.

[7] Yuni K Dewaraja, Michael Ljungberg, and Jeffrey Fessler, "3-d monte carlo-based scatter compensation in quantitative i-131 spect reconstruction," *Nuclear Science, IEEE Transactions on*, vol. 53, no. 1, pp. 181–188, 2006.

[8] Michael Ljungberg, Sven-Erik Strand, and Michael A King, *Monte Carlo calculations in nuclear medicine: Applications in diagnostic imaging*, CRC Press, 2012.

[9] WP Segars, G Sturgeon, S Mendonca, Jason Grimes, and Benjamin MW Tsui, "4d xcat phantom for multimodality imaging research," *Medical physics*, vol. 37, no. 9, pp. 4902–4915, 2010.

[10] H Malcolm Hudson and Richard S Larkin, "Accelerated image reconstruction using ordered subsets of projection data," *Medical Imaging, IEEE Transactions on*, vol. 13, no. 4, pp. 601–609, 1994.